

Hybridization of Rydberg electron orbitals by molecule formation

A. Gaj,^{*} A. T. Krupp, P. Ilzhöfer, R. Löw, S. Hofferberth, and T. Pfau[†]
 5. *Physikalisches Institut and Center for Integrated Quantum Science and Technology,*
Universität Stuttgart, Pfaffenwaldring 57, 70569 Stuttgart, Germany
 (Dated: 11 March 2015)

The formation of ultralong-range Rydberg molecules is a result of the attractive interaction between Rydberg electron and polarizable ground state atom in an ultracold gas. In the nondegenerate case the backaction of the polarizable atom on the electronic orbital is minimal. Here we demonstrate, how controlled degeneracy of the respective electronic orbitals maximizes this backaction and leads to stronger binding energies and lower symmetry of the bound dimers. Consequently, the Rydberg orbitals hybridize due to the molecular bond.

The geometrical structure of molecules determines their physical and chemical properties. The shape of an individual molecular bond can be explained by the concept of hybridization. The mixing of nearly degenerate atomic orbitals leads to a new hybrid orbital, which allows to analyze structures of many basic molecules like carbon dioxide, ammonia or water. One of the first molecules described this way is methane [1]. In CH_4 the carbon electrons, initially in s or p configuration, are rearranged into four hybrid orbitals sp^3 while creating the molecular bond. The new hybrid orbital contains 25% of s character and 75% of p character.

Here, we present the hybridization of a Rydberg electron orbital induced by the formation of an ultralong-range Rydberg molecule. Rydberg molecules consist of a single Rydberg atom bound to one or more ground state atoms. The bond in this type of molecules originates from the elastic scattering between the slow Rydberg electron and a ground state atom. Diatomic Rydberg molecules have been observed for S-states [2, 3], D-states [4, 5] and P-states [6, 7] in gases of Rb or Cs. Polyatomic Rydberg molecules have been recently photoassociated from a gas of Rb [8]. The presence of the neutral perturber inside the Rydberg electron orbital can cause admixing of a nearly degenerate hydrogenic manifold and energetically close by l -states at the location of the ground state atom [9]. As a result, these so-called trilobite molecules, can possess a giant permanent electric dipole moment. For Cs, which has an almost integer quantum defect for the S-state, this admixture can amount to 90% and lead to a permanent dipole moment of kilo-Debye, which was shown in [10] for principal quantum numbers $n=37, 39, 40$. In Rb, the hydrogenic manifold is energetically much further away. Therefore the hydrogenic admixture was less than 1% and the observed permanent dipole moments were on the order of 1 Debye for $n=35, 43$ [11]. In this paper, unlike in the experiments with trilobite states, we do not mix many states with different principal and angular quantum numbers. We demonstrate the perturber induced formation of a new hybrid orbital, which is a linear combination of only two m_j -states with known orbital shapes. For this reason, it makes it a textbook-like example of tunable hy-

bridization in the field of Rydberg molecules. The ratio of the contributing states can be precisely controlled by an applied electric field. This allows for tuning the contribution of one m_j -state to the hybrid orbital from 0 to 100% over the crossing of the two m_j -states.

In the absence of an external field, the magnetic substates of the Rydberg energy levels are degenerate. This degeneracy can be lifted by applying a magnetic field B . The initially degenerate states split then into $2j + 1$ different Zeeman levels labeled by the projection of the total angular momentum on the quantization axis m_j . Individual m_j -states can be brought back to degeneracy by applying an additional electric field \mathcal{E} aligned parallel to the B -field. In Fig. 1 calculated Stark maps in the vicinity of the $42D$ state in an external magnetic field of $B=13.55$ G are shown. The eigenenergies are obtained by diagonalizing the full Hamiltonian consisting of an unperturbed atomic Hamiltonian and two terms accounting for the interaction with the magnetic and the electric field. The splitting between states of different quantum numbers l , with $l \leq 3$ is caused by their quantum defects [12, 13]. These states exhibit a quadratic Stark effect, as can be seen for the $42D_{5/2}$ state, which splits into six m_j levels, shown in the magnification of Fig. 1. States of the manifold with $l > 3$ show a linear Stark effect, which results in a fan-like Stark structure. The magnitude of the corresponding shifts depends on the absolute value of m_j . Since the electric and magnetic dipole operators do not couple states of $\Delta m_j \neq 0$ for $\mathcal{E} \parallel B$, the $m_j=5/2$ and $m_j=1/2$ states become degenerate at $\mathcal{E}=1.135$ V/cm exhibiting real crossing. The absence of coupling between the atomic states provides a clean two level system, suitable for the investigation of hybridization of the electronic orbitals due to perturber induced coupling.

To describe the interaction of a Rydberg atom with a ground state atom in an external homogeneous electric and magnetic field, we write down the Hamiltonian:

$$H_{tot} = H_0 + H_B + H_{\mathcal{E}} + \frac{\mathbf{P}^2}{M} + V_s(\mathbf{r}, \mathbf{R}), \quad (1)$$

where $\frac{\mathbf{P}^2}{M}$ represents the kinetic energy of the ground state perturber in a center of mass frame, where M is

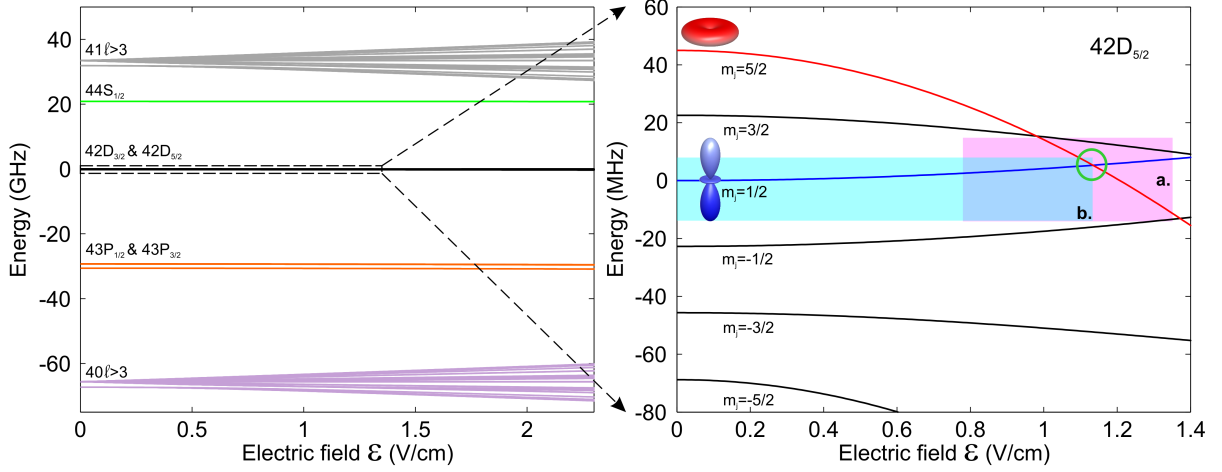


FIG. 1: Calculated Stark map in the vicinity of the $42D$ state for ^{87}Rb . The electric field is aligned parallel to the magnetic field $B=13.55\text{ G}$. All energies are plotted relative to the energy of the $42D_{5/2}, m_j = 1/2$ state at $\mathcal{E}=0$. The states are labeled with quantum numbers of the states they adiabatically unite with at $\mathcal{E}=0$. In the magnification the sixfold splitting of the $42D_{5/2}$ is shown. The green circle marks the investigated crossing of the $m_j=1/2$ (blue) and $m_j=5/2$ (red) energy levels. The part of the spherical harmonics that is relevant for the molecule formation at $\mathcal{E}=0$ is depicted close to the corresponding levels. The shaded areas a. (magenta) and b. (light blue) correspond to the measurement ranges of Fig. 2.

the reduced mass, H_0 is a field-free electron Hamiltonian and H_B and $H_{\mathcal{E}}$ account for the interaction with the electric and magnetic field, respectively. In this approach the total three body system is described by two relative positions \mathbf{R} of the ground state atom and \mathbf{r} of the electron, taken with respect to the Rydberg ionic core as well as the respective momenta \mathbf{P} and \mathbf{p} . Additionally, particles are treated as point-like. The pseudopotential $V_s(\mathbf{r}, \mathbf{R})$ describing the interaction between the low-energy electron and the perturbing atom takes, in the s -wave regime, the form [14]

$$V_s(\mathbf{r}, \mathbf{R}) = \frac{2\pi\hbar^2 a_s}{m_e} \delta(\mathbf{r} - \mathbf{R}), \quad (2)$$

where a_s is the s -wave scattering length and m_e is the electron mass. For ^{87}Rb the triplet scattering length is negative and as a consequence the potential (2) is attractive. Taking into account the local electron density, the resulting potential is proportional to $|\Psi(\mathbf{R})|^2$ [9]. Its modification due to the p -wave shape resonance can result in a binding by internal quantum reflection [15] and in the creation of butterfly-type molecules [16]. Momentum-dependent corrections to the scattering length can be calculated using a semiclassical approximation [17]. We apply a Born-Oppenheimer approximation and express the total wavefunction as $\Psi(\mathbf{r}, \mathbf{R}) = \psi(\mathbf{r}, \mathbf{R})\phi(\mathbf{R})$, where $\psi(\mathbf{r}, \mathbf{R})$ is the electronic molecular wavefunction in the presence of the perturber and $\phi(\mathbf{R})$ describes the molecular rovibrational state. This allows for computing the adiabatic potential energy surfaces (APES) for the fine structure states. Subsequently, one can calculate the molecular binding energies and the rovibrational molecular wavefunctions by solving

the Schrödinger equation using the previously calculated APES. This method was used before for theoretical studies of molecules in external magnetic and electric fields [18–20] and was experimentally verified in [4].

Here, we are interested in the mixing of two orbitals $m_j=5/2$ and $m_j=1/2$ due to the presence of the neutral atom inside the Rydberg electron orbit, which manifests itself in a change of the molecular binding energy E_B . We treat the molecular potential $V_s(\mathbf{r}, \mathbf{R})$ as a perturbation in first order to the Hamiltonian $H' = H_0 + H_B + H_{\mathcal{E}}$. For the calculation of the full Hamiltonian we use the basis of $42D_{5/2}, m_j=5/2$ and $42D_{5/2}, m_j=1/2$ electron wavefunctions

$$\begin{aligned} \psi_{1/2}(\mathbf{r}) &= R_{42D}(\mathbf{r}) Y_{1/2}(\Theta) = \sqrt{\frac{3}{5}} R_{42D}(\mathbf{r}) Y_2^0(\Theta) \\ \psi_{5/2}(\mathbf{r}) &= R_{42D}(\mathbf{r}) Y_{5/2}(\Theta, \phi) = R_{42D}(\mathbf{r}) Y_2^2(\Theta, \phi), \end{aligned} \quad (3)$$

where we include the respective Clebsch-Gordan coefficients and the spherical harmonics (shown in Fig. 2) in accordance to triplet state of the electron involved. The radial wavefunctions are the same for both states. Since we take the unperturbed wavefunctions as a basis, there is no dependence on \mathbf{R} left. Consequently, we obtain the full Hamiltonian

$$H = \eta \begin{pmatrix} |Y_{1/2}|^2 + \Delta_1/\eta & Y_{1/2}^* Y_{5/2} \\ Y_{1/2} Y_{5/2}^* & |Y_{5/2}|^2 + \Delta_2/\eta \end{pmatrix}, \quad (4)$$

where $\eta = \eta(\mathbf{R}) = \int d\mathbf{r} V_s(\mathbf{r}, \mathbf{R}) |R_{42D}(\mathbf{r})|^2$ and Δ_1 and Δ_2 are the summed-up energy shifts arising from H' . By diagonalizing the Hamiltonian (4) we obtain the new eigenenergies of the system. The degeneracy between the basis states occurs for $\Delta_1 = \Delta_2$. In the experiment we

can control the energy difference $\Delta_1 = \Delta_2 - \Delta_2$ and thus the states mixing by tuning the electric field.

We excite Rydberg atoms in a two-photon process from a magnetically trapped spin-polarized ultracold cloud of ^{87}Rb atoms in the $5S_{1/2}, F=2, m_F=2$ state [21] with an applied magnetic offset field of $B=13.55$ G. The typical temperature of the cloud is $2\text{ }\mu\text{K}$ and the peak density is on the order of 10^{12} cm^{-3} . The 780nm laser drives the lower transition. The detuning from the intermediate $5P_{3/2}$ state is 500 MHz. The 480nm laser driving the upper transition is on constantly. After each $50\text{ }\mu\text{s}$ long 780nm laser pulse we ionize Rydberg atoms and molecules with an electric field and detect the ions on a microchannel plate detector. We perform 800 cycles of excitation, ionization and detection in one cloud while scanning the frequency of the red laser. This way we obtain one full spectrum of the Rydberg signal for a given value of the electric field. We adjust the polarization of the light driving the upper transition such that the intensities of the two atomic lines close to the crossing (Fig. 1) are comparable.

In Fig. 2 we show the measured Stark maps in the vicinity of the $m_j=5/2$ and $m_j=1/2$ atomic states' crossing, marked in Fig. 1 by the green circle. Due to stray electric fields present in the experiment, the electric and magnetic field are not perfectly parallel. The angle between \vec{E} and \vec{B} is on the order of a few degrees, which in principle results in a very small coupling between the two atomic states. Nevertheless, given the resolution of our experiment, the considered atomic states appear as a true crossing. The molecular states are shifted to the red with respect to the atomic line. This energy difference corresponds to the molecular binding energy E_B . Therefore, we can identify the molecular states by comparing their binding energies with the calculated values [4] from tracing them back to the zero electric field (Fig. 2b). The molecular state visible in the Fig. 2a originates from a ground state toroidal molecule bound in the equatorial plane ($\Theta = \pi/2$) of the $m_j=1/2$ scattering potential (see inset of Fig. 1) with $E_B=3.6\text{ MHz}$ at $\mathcal{E}=0$. The molecular ground state bound in the axial lobe ($\Theta = \pi, 0$) of the same scattering potential occurs at $E_B=13.7\text{ MHz}$. This axial molecule follows in parallel the trace of the $m_j=1/2$ atomic line up to the degeneracy point, whereas the toroidal bends around the crossing and asymptotically follows the $m_j=5/2$ atomic line. In the experiment we are able to address the individual rovibrational molecular states visible in the Fig. 2b. However, since the excited toroidal states are blurred around the atomic degeneracy, we focus our analysis on the molecular ground states.

Assuming no hybridization, the molecular states of the $m_j=1/2$ and $m_j=5/2$ would occur at a constant binding energy $E_B(\mathcal{E}=0)$ with respect to the corresponding atomic lines regardless of the applied electric field. In Fig. 2 such unperturbed ground state toroidal molecule

traces, plotted in reference to the calculated atomic energy levels, are shown for the $m_j=1/2$ and $m_j=5/2$ states with continuous brown and magenta lines, respectively.

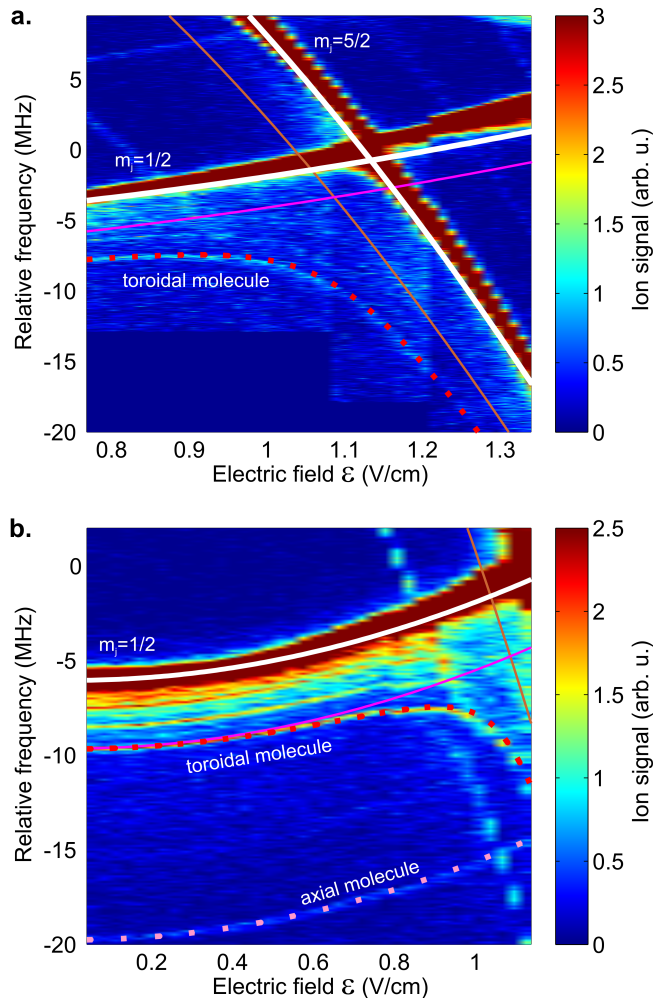


FIG. 2: Stark map in the vicinity of (a.) the degeneracy of the two atomic lines $m_j=5/2$ and $m_j=1/2$ and (b.) the $m_j=1/2$ state followed from the zero electric field up to the crossing. Computed atomic states positions, shown before in Fig. 1 are depicted with continuous white lines. All theoretical molecular lines are plotted with respect to these atomic energy levels. The hypothetical positions of the ground state toroidal molecular states, with no hybridization of the electron orbital, are indicated with brown and magenta lines, for $m_j=5/2$ and $m_j=1/2$, respectively. The binding energy of the toroidal molecule belonging to the $m_j=1/2$ state changes in the vicinity of the atomic crossing. Calculated positions of the ground state toroidal and axial molecules are indicated, for the sake of visibility, with red and pink dotted lines, respectively. In addition excited rovibrational toroidal states are visible in b. However, it is not possible to accurately trace them for higher electric fields. We identify the weak diagonal lines visible at higher electric field as laser sidebands with no physical meaning. Note that the atomic lines are saturated due to the chosen color scale. The discontinuity in the $m_j=1/2$ atomic line above 1.2 V/cm is an experimental artifact.

These two states, described by the wavefunctions (3), form a basis for our two level model. Consequently to predict the behavior of the perturbed hybrid states, we calculate the eigenenergies E_{\pm} of the Hamiltonian (4). For a given molecular state, the obtained analytical solution depends only on the energy difference Δ between the $m_j=1/2$ and $m_j=5/2$ states and a parameter η , which is determined from the fitting of E_{+} to the experimental data at $\mathcal{E}=0$. In the experiment the energy difference Δ around the crossing depends to a good approximation linearly on the electric field. E_{-} , which would correspond to the toroidal molecule of the $m_j=5/2$ state was not observed in this experiment. By calculating E_{+} , i.e. the binding energy, as a function of $\Delta(\mathcal{E})$, we reproduce the behavior of the toroidal and axial molecular lines (Fig. 2) with high accuracy. Note that the modeled molecular traces are plotted with respect to the computed atomic positions. The scattering potential couples the unperturbed toroidal molecular lines, although the respective atomic states cross without any level repulsion between them. This leads to orbital mixing and therefore a change in the Rydberg electron probability density, which we observe as an increased binding energy of the toroidal molecule. In case of the axial molecule, the off diagonal coupling terms in the Hamiltonian (4) vanish. This is due to the fact that the torus-like $m_j=5/2$ spherical harmonic is zero along the axial direction and thus does not modify the $m_j=1/2$ state in this direction. For this reason the binding energy stays constant.

In Fig. 3 the measured and calculated (E_{+}) binding energies of the considered molecules versus the electric field are shown. Here the binding energy is determined as the difference between the measured atomic and molecular energy. The binding energy of the toroidal molecules increases from $E_B(\mathcal{E}=0)$ of the $m_j=1/2$ state, reaches its maximum of $E_B=11.7$ MHz and asymptotically decreases to $E_B(\mathcal{E}=0)$ of the $m_j=5/2$ state. This transition can be attributed to an increase of the admixture of the $m_j=5/2$ state from 0 to 100%. The maximum binding energy corresponds to an orbital consisting of 50% $m_j=1/2$ character and 50% $m_j=5/2$ character. The resulting shape of the orbital is shown in the inset of Fig. 3. The hybridization introduces a ϕ -dependence to the Rydberg orbital, even though the asymptotic states were spherically symmetric along the z -axis. For the unperturbed axial molecule, the shape of the Rydberg orbital remains the same.

Directly at the crossing the experimental binding energy of the toroidal molecule and the calculated one deviate by 9%. The predominant reason of the discrepancy around the crossing, for $\mathcal{E} > 0.8$ V/cm, are difficulties in determining the atomic peak position caused by its non-Gaussian shape. Additionally, for $\mathcal{E} > 1.2$ V/cm fitting of the molecular state position becomes problematic. Moreover, for the calculation we only take the unperturbed states and not the real Stark states into account. Finally,

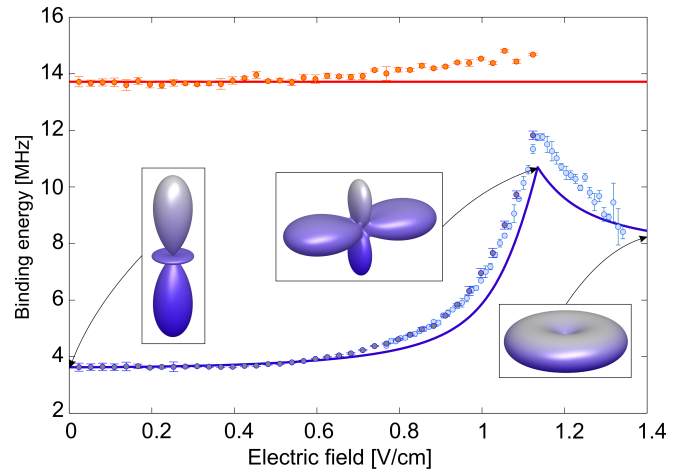


FIG. 3: Measured binding energies of the axial (orange points) and toroidal ground state molecules (light blue and violet points) versus the electric field. The binding energies are extracted from two data sets shown in Fig. 2 (a. and b.) and hence indicated with two colors for the toroidal molecule data. A ground state atom inside the Rydberg electron in the toroidal plane mixes two orbitals. As a result the binding energy of the $m_j=1/2$ toroidal molecule increases, reaches its maximum directly at the crossing and then asymptotically decreases to the E_B value of $m_j=5/2$ toroidal molecule. The relevant part for molecule formation of the spherical harmonic of the hybridized Rydberg orbital at the crossing is shown in the inset together with the two asymptotic shapes. The error bars are determined as two standard deviations of the fit.

more levels could be included into the analysis. In view of these facts, the agreement between the experimental data and our simple model is remarkable. A more complicated analysis would not lead to a significantly better agreement due to the purely experimental constraints.

We have shown the hybridization of the Rydberg electron orbital due to the molecule formation around the crossing of the atomic lines $m_j=1/2$ and $m_j=5/2$. The backaction of the bound perturber increases the binding energy and consequently changes the shape of the electron orbital. Mixing more than two electron orbitals of known shapes by bringing them to degeneracy could result in even more complex asymmetric electron configurations. Furthermore, the influence of a different type of perturber, like an atom of another element or a heteronuclear molecule [22], as well as the effect of a few perturbors on the electron orbital could be investigated. Rydberg electron orbital hybridized due to thousands of the ground state perturbors could be observed as an imprint on a Bose Einstein condensate [23]. Finally, engineering a state by placing the perturber precisely at a desired position might also be feasible in experiments with individual atoms in microtraps.

We acknowledge support from the Deutsche Forschungsgemeinschaft (DFG) within the SFB/TRR21 and the project PF 381/13-1. Parts of this work was

also funded by the ERC under contract number 267100. A.G. acknowledges support from the E.U. Marie Curie program ITN-Coherence 265031 and S.H. from DFG through the project HO 4787/1-1. A.G. and A.T.K. contributed equally to this work.

* Electronic address: a.gaj@physik.uni-stuttgart.de

† Electronic address: t.pfau@physik.uni-stuttgart.de

- [1] L. Pauling, *Journal of the American Chemical Society* **53**, 1367 (1931).
- [2] V. Bendkowsky, B. Butscher, J. Nipper, J. P. Shaffer, R. Löw, and T. Pfau, *Nature* **458**, 0028 (2009).
- [3] J. Tallant, S. T. Rittenhouse, D. Booth, H. R. Sadeghpour, and J. P. Shaffer, *Phys. Rev. Lett.* **109**, 173202 (2012).
- [4] A. T. Krupp, A. Gaj, J. B. Balewski, P. Ilzhöfer, S. Hofferberth, R. Löw, T. Pfau, M. Kurz, and P. Schmelcher, *Phys. Rev. Lett.* **112**, 143008 (2014).
- [5] D. A. Anderson, S. A. Miller, and G. Raithel, *Phys. Rev. Lett.* **112**, 163201 (2014).
- [6] M. A. Bellos, R. Carollo, J. Banerjee, E. E. Eyler, P. L. Gould, and W. C. Stwalley, *Phys. Rev. Lett.* **111**, 053001 (2013).
- [7] H. Saßmanhausen, F. Merkt, and J. Deigmayer, *arXiv:1412.0846v2* (2014).
- [8] A. Gaj, A. T. Krupp, J. B. Balewski, R. Löw, S. Hofferberth, and T. Pfau, *Nature Comm.* **5** (2014).
- [9] C. H. Greene, A. S. Dickinson, and H. R. Sadeghpour, *Phys. Rev. Lett.* **85**, 2458 (2000).
- [10] D. Booth, S. Rittenhouse, J. Yang, H. Sadeghpour, and J. Shaffer, *arXiv:1411.5291* (2014).
- [11] W. Li, T. Pohl, J. M. Rost, S. T. Rittenhouse, H. R. Sadeghpour, J. Nipper, B. Butscher, J. B. Balewski, V. Bendkowsky, R. Löw, et al., *Science* **334**, 1110 (2011).
- [12] W. Li, M. Mourachko, M. W. Noel, and T. F. Gallagher, *Phys. Rev. A* **67**, 052502 (2003).
- [13] M. Mack, F. Karlewski, H. Hattermann, S. Höckh, F. Jessen, D. Cano, and J. Fortagh, *Phys. Rev. A* **83**, 052515 (2011).
- [14] E. Fermi, *Nuovo Cimento* **11**, 157 (1934).
- [15] V. Bendkowsky, B. Butscher, J. Nipper, J. B. Balewski, J. P. Shaffer, R. Löw, T. Pfau, W. Li, J. Stanojevic, T. Pohl, et al., *Phys. Rev. Lett.* **105**, 163201 (2010).
- [16] E. L. Hamilton, C. H. Greene, and H. R. Sadeghpour, *J. Phys. B: At. Mol. Opt. Phys.* **35** (2002).
- [17] A. Omont, *J. Phys. France* **38**, 1343 (1977).
- [18] I. Lesanovsky, P. Schmelcher, and H. R. Sadeghpour, *J. Phys. B: At. Mol. Opt. Phys.* **39**, L69 (2006).
- [19] M. Kurz and P. Schmelcher, *Phys. Rev. A* **88**, 022501 (2013).
- [20] M. Kurz and P. Schmelcher, *J. Phys. B: At. Mol. Opt. Phys.* **47**, 165101 (2014).
- [21] R. Löw, H. Weimer, J. Nipper, J. B. Balewski, B. Butscher, H. P. Büchler, and T. Pfau, *J. Phys. B: At. Mol. Opt. Phys.* **45**, 113001 (2012).
- [22] R. González-Férez, H. R. Sadeghpour, and P. Schmelcher, *New J. Phys.* **17**, 013021 (2014).
- [23] T. Karpiuk, M. Brewczyk, K. Rzażewski, J. B. Balewski, A. T. Krupp, A. Gaj, R. Löw, S. Hofferberth, and T. Pfau, *arXiv:1402.6875v1* (2014).